Documents

Export Date: 10 Jan 2019

Search: ALL(52864492100)

1) Hao, L.V., Koleda, A., Barbin, E., Nesterenko, T.

MEMS Instrument Accuracy in Automated Vehicle Control

(2018) Journal of Physics: Conference Series, 1118 (1), art. no. 012061, .

1) https://www.scopus.com/inward/record.uri?eid=2-s2.0-85059019821&doi=10.1088%2f1742-6596%2f1118%2f1%2f012061&par

DOI: 10.1088/1742-6596/1118/1/012061

Document Type: Conference Paper

Publication Stage: Final

Access Type: Open Access

Source: Scopus

MEMS Instrument Accuracy in Automated Vehicle Control

MEMS Instrument Accuracy in Automated Vehicle Control

Lo Van Hao[1], **Aleksey Koleda**[2], **Evgenii Barbin**[3] and **Tamara Nesterenko**[4]

Tomsk Polytechnic University, 30, Lenina ave., Tomsk, 634050, Russia

E-mail: lovanhao.pro@gmail.com[1], kopranchikos@tpu.ru[2], bares@tpu.ru[3], ntg@tpu.ru[4]

Abstract. Today, humanity faces the development of unmanned vehicles. No automated vehicle control system can be without sensors which read out data on its motion. The accuracy of unmanned vehicle motion directly depends on the instrument accuracy and applicability of sensors integrated in the automated vehicle control system. The design of such sensors should consider defects which occur during their manufacturing. The aim of this work is to study the technology component effect on the dynamic properties of a multi-axis gyroscope intended for the automated vehicle control..

1. Introduction

Transportation is highly relevant to both the population welfare and the normal functioning of the business community and the government on the whole.

Integrated navigation systems employed in the vehicle control are a well-developed up-to-date technology. The vehicle control systems have gradually become lighter, cheaper, more compact and beneficial over the past decades. The automated control for various vehicles implies the use of different sensors which determine the attitude control parameters and the dynamic properties of the object.

Motion sensors must have a low cost, small size, and the appropriate accuracy under various climate changes and mechanical perturbation impacts. Microelectromechanical (MEMS) motion sensors satisfy these requirements and underlie a composition of vehicle strapdown attitude reference and navigation systems (SARNS). The flowchart of such system is presented in Fig. 1.

The navigation management in SARNS is performed by means of self-contained aids using readings of the gyroscope, the accelerometer, and the magnetometer integrated in the inertial module [1, 2, 14]. The main disadvantage of the inertial dead-reckoning method is the error accumulation over time [3, 4, 16]. In SARNS, basic errors are produced by the inertial module and must be eliminated. Moreover, the MEMS SARNS can operate in tandem with a satellite navigation system which allows increasing the attitude control accuracy of a vehicle.

According to the marketing research conducted by the Yole Development Company [5, 15,17], the amount of multi-axis inertial motion sensors will be growing each year, and the amount of three- and less-axis motion sensors will be lowering. This is because a consumer market shifts toward multi-axis sensors which are becoming very popular in many applications which involve measuring lots of parameters. This phenomenon is linked to a rapidly growing unmanned technical and safety equipment which utilizes inertial modules as basic devices.

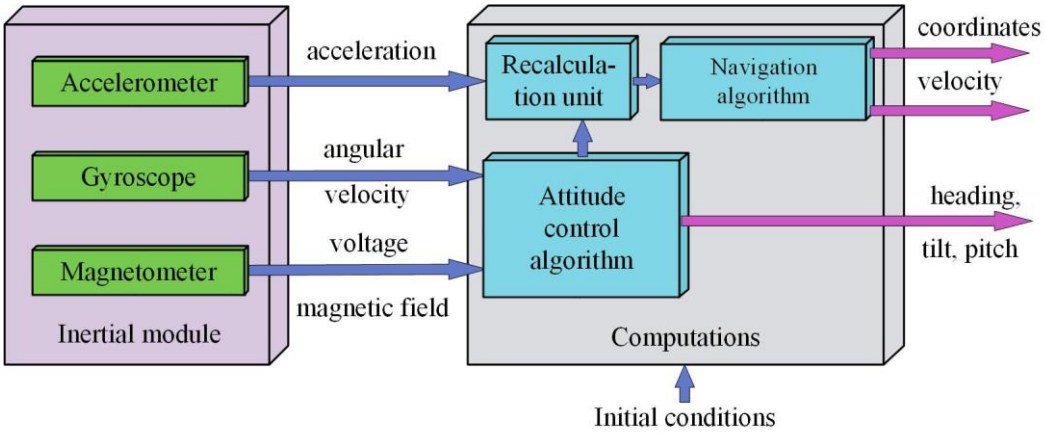

Figure 1. The flowchart of vehicle strapdown attitude reference and navigation system

MEMS sensors are therefore widely used in various civil and military equipment. The current performance requirements for MEMS sensors are constantly growing due to expanding their applications with the particularly higher level of external factors (see Fig. 2).

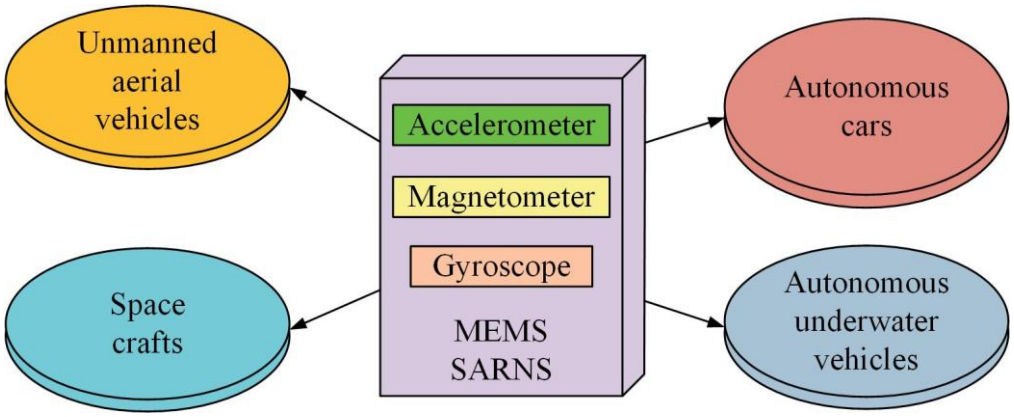

Figure 2. MEMS sensor applications

Moreover, MEMS devices possessing the accuracy factors and other performance characteristics in the extended range of parameters are needed in such application fields as hole making navigation, military engineering, construction, transportation, railway and road-transport economies. MEMS sensors must satisfy the stability requirements, i.e. maintain the workability and accuracy factors in some very tough environments.

MEMS sensors combine mechanical and electrical components of extremely small size. They should be protected from external impacts of different origins, such as physical, chemical, and mechanical. It is notable that mechanical and electrical components in MEMS sensors are made of a common plate using the technology of forming three-dimensional structures.

The high accuracy of MEMS sensors is achieved through considering such factors as physical properties of constructional materials, instrument accuracy of manufacturing sensitive elements and operating conditions and measuring accuracy of sensors [6-9], development and improvement of MEMS technology in Russia, shortening design and production periods of MEMS sensor prototypes, comprehensive examination of projects prior to the real production process using the modern electronic devices.

There are several main routes of developing the qualitative production of inertial sensors, namely: the size reduction, increase in the number of sensors in one housing, reduction of consumption, and increase in the number of smart functions.

Manufacturing of MEMS integrated sensors is a complex production process which involves rather an expensive product line. It is therefore advisable to perform a system model-building of the whole device together with its measuring circuit. This allows a developer to reduce costs and time of the MEMS sensor production.

The aim of this work is to study the technology component effect on the dynamic properties of a multi-axis gyroscope intended for the automated vehicles control.

2. Architecture and dynamic properties

A multi-axis microgyroscope (Fig. 3) is a three-component gyroscopic module, which measures three components of the angular velocity.

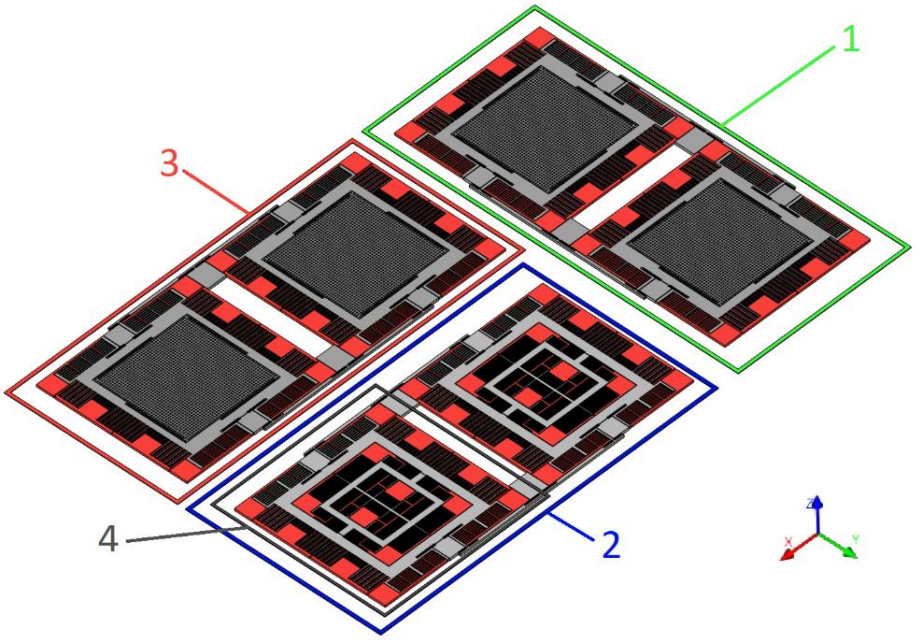

Figure 3. Silicon electromechanical sensor (SES) of three-component gyroscopic module:
1 – Y-sensor; 2 – Z-sensor; 3 – X-sensor; 4 - sensor unit

SES consists of three one-component (single-axis) microgyroscopes. A Y-sensor and an X-sensor are similar and are positioned at an angle of 90 degrees relative to each other. The third one (Z-sensor) has other architecture.

Each sensor of MEMS gyroscope contains two symmetrical sensor units adjacent to each other via a spring element. The gyroscope module comprises anti-phase systems positioned along the axes of primary oscillations. Secondary oscillations will also make anti-phase movement that allows reducing the influence of acceleration on output signal. Primary oscillations of Z- and X-sensors occur along the Y axis; the Y-sensor - along the X axis. Due to base angular velocity by means of Coriolis force, secondary oscillations of the Z-sensor occur along the X axis, X- and Y-sensors occur along the Z axis. Each sensor measures the same name components of angular velocity. Angular velocities are measured by the capacitances of the silicon sensor [10-13, 18].

3. Technology component

The mainstream technology applied in the gyroscope module microfabrication is a deep anisotropic ion etching of silicon. The manufacture of moving sensing structures is provided by a silicon-on-glass technique, the schematic diagram of which is presented in Fig. 4. A silicon sensor is mounted to the glass substrate. The electrical connection is performed via metal electrodes sprayed onto the glass substrate surface.

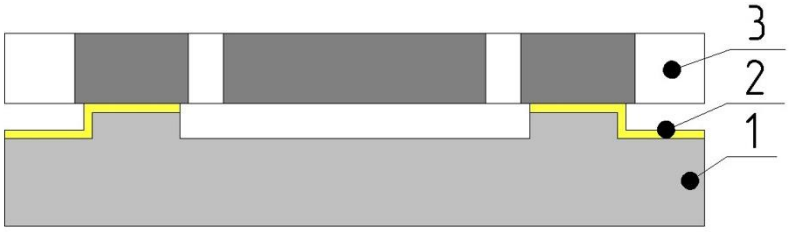

Figure 4. Schematic of silicon-on-glass technique: 1 – glass substrate; 2 – metal electrodes; 3 – silicon sensor

The substrate is made of a 20×20×0.5 mm borosilicate glass. The MEMS sensor is made of single-crystal silicon. The scanning electron microscopy (SEM) images of this sensor are presented in Fig. 5.

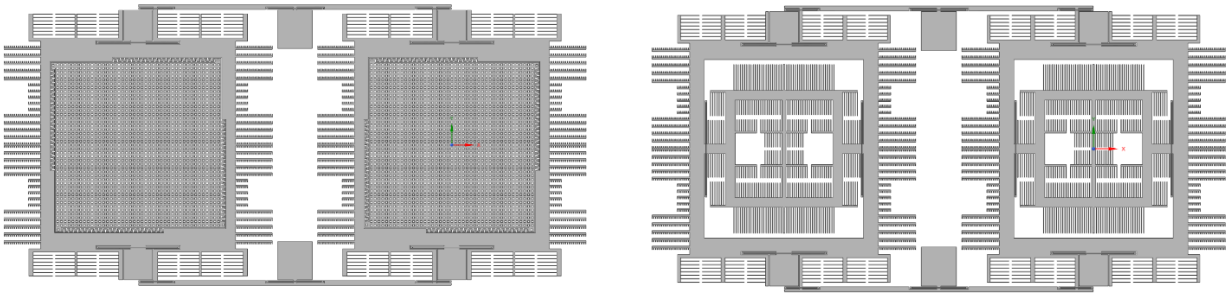

a) Y, X-sensors b) Z- sensor

Figure 5. . Single-component microscopes of three-component gyroscopic module SEM

In-process defects can occur during the photolithography and photomask fabrication and silicon etching which cause the size distortion of the silicon MEMS sensor and change its parameters. The most significant impact of in-process defects on the silicon MEMS sensor occurs due to a change in its geometry. Thus, in-process defects include ±0.1 μm size tolerance in the sensor plane (b parameter); ±0.05 μm height tolerance in the sensor plate (h parameter); vertical deviation of walls between 0–0.1 degrees (α angle). These parameters are schematically shown in Fig. 6.

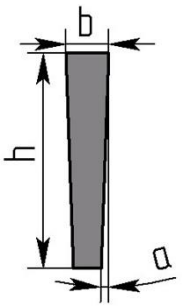

Figure 6. MEMS sensor varying parameters

Non-uniform etching causes changes in the geometry of spring elements of frames, thereby affecting the sensor eigen-frequency and, as a consequence, the scaling factor of the MEMS gyroscope. Therefore, the effect produced by the silicon etching on the gyroscope dynamic properties should be evaluated as early as at a design stage using the finite element analysis.

During the analysis of the instrument accuracy, one of the investigated parameters is changed, all other parameters being constant. A ±0.1 μm change in the linear sizes along Y- and X-axes is characteristic to b parameter depicted in Fig. 7.

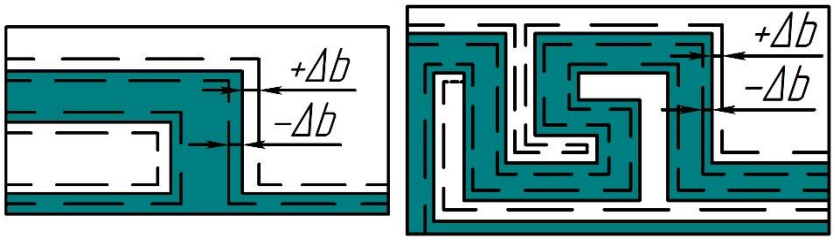

Figure 7. MEMS sensor varying parameters

Figure 8 presents a block-diagram for the in-process defects which change the silicon MEMS sensor parameters. Thus, a change in the b parameter by 100 nm modifies the eigen-frequency by 79 Hz. A change in the h parameter by 50 nm causes a 53 Hz change in the eigen-frequency. And a change in α parameter by 0.1 degrees enables the eigen-frequency to change by 103 Hz (Fig. 8).

The scaling factor of the MEMS gyroscope changes respectively by 3, 0.8 and 8 %, when changing b, h and α parameters by 100 nm, 50 nm, and 0.1 degrees, respectively. Such cases are depicted in Fig. 9.

The dependences between the scaling factors and b parameter of the silicon MEMS sensor can be approximated by the following equations:

$$\begin{aligned} k_x(b) &= 2.55 \cdot 10^{-10} - 0.00022781916 \cdot b, \\ k_y(b) &= 2.54 \cdot 10^{-10} - 0.00022164233 \cdot b, \\ k_z(b) &= 2.54 \cdot 10^{-10} - 0.00019876024 \cdot b. \end{aligned} \quad (1)$$

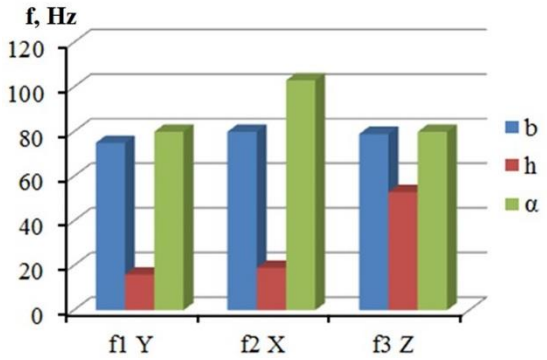

Figure 8. Eigen-frequency of silicon MEMS sensor depending on b, h, α parameters

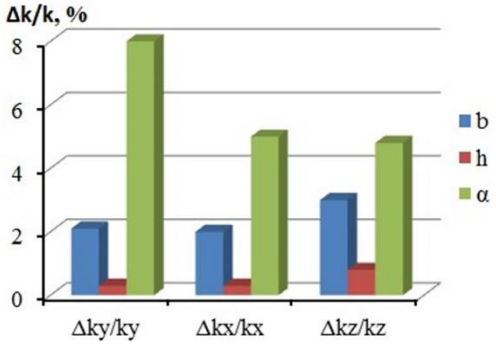

Figure 9. Relative dependences of silicon MEMS sensor scaling factors depending on b, h, α parameters

The dependences between the scaling factors and h parameter of the silicon MEMS sensor can be approximated by the following equations:

$$k_x(h) = 2.55 \cdot 10^{-10} - 8.65 \cdot 10^{-7} \cdot h,$$
$$k_y(h) = 2.55 \cdot 10^{-10} - 4.08 \cdot 10^{-7} \cdot h, \quad (2)$$
$$k_z(h) = 2.54 \cdot 10^{-10} - 1.22 \cdot 10^{-7} \cdot h.$$

The dependences between the scaling factors and α parameter of the silicon MEMS sensor can be approximated by the following equations:

$$k_x(\alpha) = 2.55 \cdot 10^{-10} + 8.91 \cdot 10^{-11} \cdot \alpha,$$
$$k_y(\alpha) = 2.54 \cdot 10^{-10} + 1.17 \cdot 10^{-10} \cdot \alpha, \quad (3)$$
$$k_z(\alpha) = 2.54 \cdot 10^{-10} + 7.64 \cdot 10^{-11} \cdot \alpha.$$

Capacitances of the electrode structures also depend on the geometry of comb electrode structures. So it is expedient to evaluate these dependences induced by the in-process defects. The block diagram in Fig. 10 indicates the impact of in-process defects on capacitances C1y and C2y along the axis of primary oscillations.

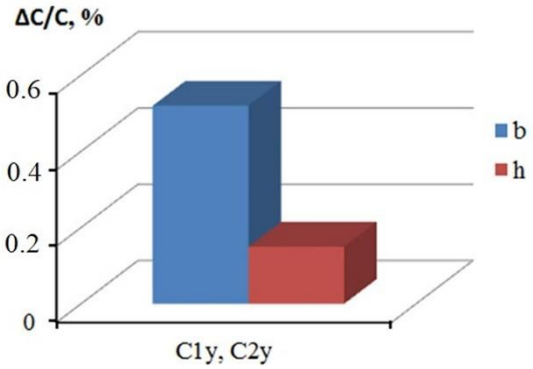

Figure 10. Relative dependence of capacitances C1y and C2y on b and h parameters along the axes of primary oscillations

As can be seen from Fig. 10, the comb electrodes underetching reduces the b parameter, which causes a 0.52% reduction of capacitances. A change in the h parameter results in the reduction of capacitances by 0.15%.

The block diagram in Fig. 11 indicates the impact of in-process defects on capacitances C1y and C2y of sensing electrodes.

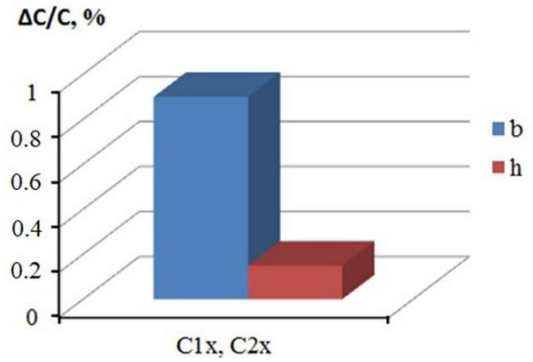

Figure 11. Relative dependence of sensing electrodes capacitances C1y and C2y on b and h parameters

According to Fig. 11, a change in the b parameter by 100 nm results in the comb electrodes underetching which, in turn, causes the reduction in their size and the 0.9% reduction in capacitances. When the h parameter is changed by 50 nm, the height of comb electrodes also changes, thereby causing a 0.15% decrease in capacitances.

The block diagram in Fig. 12 indicates the impact of in-process defects on capacitances C3y and C4y along the axes of primary oscillations.

Figure 12 shows that a change in the b parameter by 100 nm results in the comb electrodes underetching which, in turn, causes the reduction in their size and 3% reduction in capacitances. When the h parameter is changed by 50 nm, the height of comb electrodes also changes, thereby causing a 0.42% decrease in capacitances.

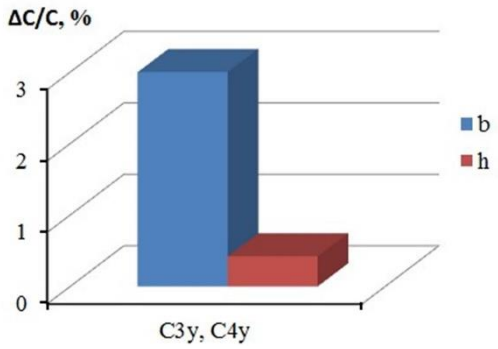

Figure 12. Relative dependence of capacitances C3y and C4y on b and h parameters along the axes of primary oscillations

4. Conclusion

In conclusion, it is evident that in-process defects had a random character and depended on a certain model of instrument used in the production process. As a result of the finite element analysis, the instrument accuracy dependences were suggested for frequencies, scaling factors and capacitances. The obtained dependences were used to compensate in-process defects which affect the performance parameters of the integrated MEMS gyroscopes.

In computer simulation of the photomask, the compensation of in-process defects, which occurred during its fabrication, was achieved through rounding sharp edges and corners of diverse model elements by 1 micron. As a result, the defect was reduced down to 0.004 μm. In order to eliminate in-process defects, the model size was reduced by 0.1 microns.

When silicon was etched at a depth of 40 μm, the appeared underetching defect was eliminated by a change in the hardware configuration, i.e. we set the etching time such that etching did not exceed 0.1 μm.

5. Acknowledgments

This work was performed in National Research Tomsk Polytechnic University. The authors would like to acknowledge the financial support of the Ministry of Education and Science of the Russian Federation (Agreement № 14.578.21.0232, unique identifier RFMEFI57817X0232).

References

[1] Baranova V E, Baranov P F, Muravyov S V, and Uchaikin S V 2015 The Production of a Uniform Magnetic Field Using a System of Axial Coils for Calibrating Magnetometers, *Measurement Techniques* **58(5)** 550–555

[2] Kolomeytsev A, Baranov P, and Zatonov I 2018 The Fluxgate Magnetometer Simulation in Comsol Multiphysics *MATEC Web of Conf.* **155**

[3] Eminoglu B et al 2016 Comparison of long-term stability of AM versus FM gyroscopes, *Proceedings of the IEEE International Conference on Micro Electro Mechanical Systems* **2016** 954–957

[4] Dehghani M, Kharrati H, Seyedarabi H, and Baradarannia M 2018 Improvement of angular velocity and position estimation in gyro-free inertial navigation based on vision aid equipment, *IET Computer Vision* **12(3)** 261–275

[5] Retrieved from: http://www.yole.fr.

[6] Dzhashitov V E, Pankratov V M, Barulina M A, and Golikov A V 2010 *Prospects for the development and creation of superminiature micromechanical multipurpose sensors of inertial*

information, 17th Saint Petersburg International Conference on Integrated Navigation Systems, ICINS 2010 – Proceedings, pp. 48–53

[7] Cao H, Li H, Sheng X, Wang S, Yang B, and Huang L 2013 A novel temperature compensation method for a MEMS gyroscope oriented on a periphery circuit, *International Journal of Advanced Robotic Systems* **10**

[8] Tatar E, Alper S E, and Akin T 2012 Quadrature-error compensation and corresponding effects on the performance of fully decoupled MEMS gyroscopes, *Journal of Microelectromechanical Systems* **21(3)** 656–667

[9] Tsai C-W, Chen K-H, Shen C-K, and Tsai J-C 2012 A MEMS doubly decoupled gyroscope with wide driving frequency range, *IEEE Transactions on Industrial Electronics* **59(12)** 4921–4929

[10] Zorina E V, Nesterenko T G, Baranov P F, Koleda A N and Barbin E S 2016 New architecture and configuration of microelectromechanical acceleration, *Procedia Engineering* 168 904–907

[11] Nasonov M Y, Lykov Y V 2017 Setting up excavators with growing cracks in their metal structures for repairs. *IOP Conference Series: Earth and Environmental Science* **87** 022015

[12] Belyaev A I, Afanasyev A S 2016 Efficiency of Vehicle Operation. *International Journal of Economics and Financial Issies* **6(S3)** 1-7

[13] Davydenko M I, Yaroslavova Yu E, Nazarova M N 2017 Analysis of emergence polyethylene piplenes depending on the method installation Geonature 2017 *European Association of Geoscientists and Engineers (EAGE),* pp. 294-297

[14] Ershov D Y, Zlotnikov E G, Koboyankwe L E 2017 Dynamic processes in technological systems of machining and the nature of their origin. *IOP Conference Series: Earth and Environmental Science* **87(8)** 82016

[15] Yungmeister D A, Kireev K A 2016 Development of the construction and characterization of deep complex for collecting imc. *Research Journal of Pharmaceutical, Biological and Chemical Sciences* **7(2)** 2086-2091

[16] Demidovich V B, Rastvorova I I 2014 Combined Method of Simulation of Electric Circuit and Field Problems in the Theory of Induction Heating. *Russian Electrical Engineering* **85-8** 536-540

[17] Maksarov V V, Krasnyy V A, Viushin R V 2018 Simulation of dynamic processes when machining transition surfaces of stepped shafts. *IOP Conf. Series: Materials Science and Engineering* **327** 022047 doi:10.1088/1757-899X/327/2/022047

[18] Nguyen K L, Gabov V V, Zadkov D A, Le T B 2018 Justification of process of loading coal onto face conveyors by auger heads of shearer-loader machines. *IOP Conference Series: Materials Science and Engineering* **327** 042132 doi:10.1088/1757-899X/327/4/042132